THE HISTORY OF THE MYSTERIOUS ECLIPSES OF KH 15D: ASIAGO OBSERVATORY, 1967–1982[1]

JOHN ASHER JOHNSON[2] AND JOSHUA N. WINN[3,4]

ABSTRACT

We are gathering archival observations to determine the photometric history of the unique and unexplained eclipses of the pre–main-sequence star KH 15D. Here we present a light curve from 1967 to 1982, based on photographic plates from Asiago Observatory. During this time, the system alternated periodically between bright and faint states, as observed today. However, the bright state was 0.9 mag brighter than the modern value, and the fractional variation between bright and faint states ($\Delta I = 0.7$ mag) was smaller than observed today (3.5 mag). A possible explanation for these findings is that the system contains a second star that was previously blended with the eclipsing star but is now completely obscured.

Key words: circumstellar matter — open clusters and associations: individual (NGC 2264) —
stars: individual (KH 15D) — stars: pre–main-sequence — techniques: photometric

1. INTRODUCTION

Pre–main-sequence stars are well known for their photometric variability, both erratic and periodic (see, e.g., Herbst et al. 1994). However, the photometric behavior of KH 15D is unusual even by the standards of pre–main-sequence stars. The star is a 2–10 Myr old T Tauri star of spectral type K7, located in the open cluster NGC 2264 (Hamilton et al. 2001). As discovered by Kearns & Herbst (1998), the star's brightness decreases by 3.5 mag every 48.35 days, and these deep brightness excursions currently last more than 20 days. The extreme depth and long duration of the eclipses rule out occultation by a companion star, or modulation by starspots, as a possible explanation. The strict periodicity seems incompatible with a mechanism based on unstable accretion. During brightness minima the fractional polarization rises, suggesting that the entire face of the star is occulted by circumstellar material and that only scattered light is received at those times (Agol et al. 2004). It is hoped that continued observations will reveal the geometry and structure of the material and provide unique information about circumstellar processes, or even planet-forming processes.

The brightness variations are not accompanied by significant color variations (Herbst et al. 2002), implicating large particles or macroscopic bodies as the occulters. The ingress and egress light curves can be understood qualitatively as the result of a sharp occulting edge moving across the face of the star with a velocity vector nearly parallel to the edge. A peculiar phenomenon observed at mid-eclipse is the "central rebrightening": a phase lasting a few days during which the star rebrightens. In the past, the central rebrightening returned the system brightness to the out-of-eclipse level. In one early observation, the star *exceeded* its uneclipsed brightness by 0.5 mag (Hamilton et al. 2001).

Ongoing photometric monitoring by Hamilton et al. (2001) and Herbst et al. (2002) has shown that the light curve of KH 15D evolves with time. The duration of the eclipses has been growing steadily since 1996, at a rate of ≈ 1 day yr^{-1}. The central rebrightenings have been declining in maximum flux and are now much less pronounced than they used to be. Given these secular changes, it should be illuminating to assemble a historical light curve of KH 15D from archival photographic observations of NGC 2264. Fortunately, it is realistic to expect that suitable archival observations exist. The star is presently bright enough ($V = 16$) to have been detected on photographic plates with modestly sized telescopes. It resides in a young and relatively unobscured cluster full of variable stars that has attracted scientific interest for many decades.

Winn et al. (2003) performed the first archival study of KH 15D, using plates from the collection of the Harvard College Observatory. Although the star was too faint and too blended with a nearby bright star for accurate photometry, Winn et al. established that between 1913 and 1955 the star was rarely (if ever) fainter by more than 1 magnitude than its present uneclipsed state. They expressed this result as an upper limit of 20% on the duty cycle of 1 mag eclipses.

This showed that the deep eclipses are a recent phenomenon and motivated the search for more photographs taken after 1950 in order to identify the onset of the eclipses. We have been gathering additional plates from observatories around the world in order to fill in the photometric history of KH 15D. This paper presents new results from our archival exploration, based on a time series of high-quality photographic plates from the Asiago Observatory, taken between 1967 and 1982. In § 2, we describe the plates and the digitization process. We determined the magnitude of KH 15D on each plate with the procedure described in § 3. The Asiago light curve is presented in § 4 and compared with the modern light curve. We conclude in § 5 by summarizing the results and speculating on the reason for the striking evolution of the system between 1967 and today.

2. SELECTION AND DIGITIZATION OF THE PLATES

The Astrophysical Observatory of Asiago,[5] in northern Italy, houses a collection of nearly 80,000 photographic plates

[2] Department of Astronomy, University of California at Berkeley, Berkeley, CA 94720-3411; johnjohn@astron.berkeley.edu.
[3] Harvard-Smithsonian Center for Astrophysics, 60 Garden Street, Cambridge, MA 02138; jwinn@cfa.harvard.edu.
[4] National Science Foundation Astronomy and Astrophysics Postdoctoral Fellow.

[5] See http://www.pd.astro.it/asiago/.

(Barbieri, Omizzolo, & Rampazzi 2003). Among them are more than 300 images of NGC 2264, but most of the exposures were too shallow to expect KH 15D to be detectable. In some other cases, the exposure is sufficiently deep but the position of KH 15D is excessively contaminated by the extended halo of scattered light from a nearby bright B star, HD 47887. This was also the main problem with the Harvard plates (Winn et al. 2003).

All the plates described in this paper were obtained with the 92/67 cm Schmidt telescope at the Cima Ekar station of Asiago Observatory, between 1967 and 1982. We found 48 plates with reasonably long, red-sensitive exposures that were ideally suited for our study. These were exposed with a I-N emulsion and RG 5 filter. The I-N emulsion was designed for improved sensitivity redward of typical astronomical emulsions, to a cutoff near 9200 Å (Stock & Williams 1962). The long-pass RG 5 filter is identical to the modern RG 665 Schott filter and blocks wavelengths shorter than 6400 Å. Together, the I-N/RG 5 combination has a transmission curve similar to the ≈7000–9000 Å bandpass of the Cousins *I* band.

Although the plates with bluer sensitivity were not as well suited for photometry, we still wanted to get at least some color information. For this reason, we also searched for a few high-quality examples. We selected three plates exposed with a 103a-E emulsion and RG 1 filter, which together have a spectral response similar to the Johnson *R* band (Moro & Munari 2000). We also selected one plate exposed with a 103a-O emulsion and GG 5 filter, giving a spectral response similar to the Johnson *B* band. The contents of our Asiago sample can be summarized as 48 *I*-like plates, three *R*-like plates, and one *B*-like plate. These fall into three groups in time, with 41 plates taken from 1967 to 1970, six plates from 1973 to 1976, and five plates from 1979 to 1982.

We digitized these plates at Asiago Observatory using a commercial flatbed scanner with a resolution of 1600 dots per inch and a dynamic range of 14 bits pixel^{-1}. The pixel scale of the digitized images is 1″53 pixel^{-1}. Given that the typical seeing was 6″–9″, the digitized stellar images have a full width at half-maximum of 4–6 pixels. The entire $5° \times 5°$ field of view was scanned, but for our analysis we extracted a $20' \times 20'$ subraster centered on HD 47887. A sample digitized image is shown in Figure 1.

3. PHOTOMETRY

Astronomical photographic emulsions used throughout the last century typically consisted of a suspension of silver halide in a substrate of gelatin (Stock & Williams 1962). When light strikes the halide, it produces a distribution of metallic silver grains that is made permanent by chemical development and fixation. The challenge of photographic stellar photometry is to relate the spatial distribution of the grains in a stellar image to the flux of the star.

The scanner measures $T(x, y)$, the fraction of transmitted light as a function of position on the plate. What is actually recorded is the "density distribution,"

$$d(x,y) = 2^{N_{\rm bit}}[1 - T(x,y)], \qquad (1)$$

where $N_{\rm bit} = 14$ is the number of bits per pixel in the digitized image. The relationship between $d(x, y)$ and stellar flux is nonlinear. In particular, for intensities above some threshold value, the density saturates. The following sections describe our method to correct for the effects of nonlinearity and
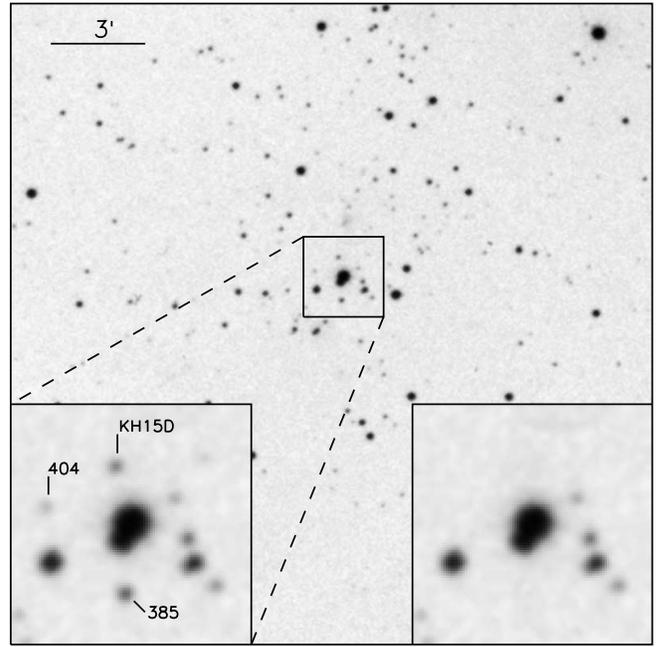

FIG. 1.—Digitization of a I-N/RG 5 plate from 1968 January 21. North is up and east is to the left. The field of view is $20' \times 20'$, centered on the bright star HD 47887. Insets in the corners are close-ups of the region surrounding HD 47887, showing KH 15D and two of the reference stars before and after subtracting the point-spread function model (eq. [4]).

saturation, and to calibrate the magnitude of KH 15D using a system of local reference stars on each plate.

3.1. *Point-Spread Function Fitting*

Our first step was to fit a parametric model to the density distribution of each star. The density distribution of faint stars is well described by a two-dimensional Gaussian function,

$$d_{\rm G}(x,y) = d_{\rm sky} + \frac{d_{\rm peak}}{2\pi\sigma_x\sigma_y\sqrt{1-\rho^2}} \exp\left[-\frac{z^2}{2(1-\rho^2)}\right], \qquad (2)$$

where ρ parameterizes the rotation and the dimensionless elliptical coordinate z is defined via the equation

$$z^2 = \frac{(x-x_0)^2}{\sigma_x^2} - \frac{2\rho(x-x_0)(y-y_0)}{\sigma_x\sigma_y} + \frac{(y-y_0)^2}{\sigma_y^2}. \qquad (3)$$

In contrast, bright stars have a flat-topped density distribution, due to saturation. The top two panels of Figure 2 show the density distributions of a bright star ($I \sim 9$) and the much fainter KH 15D, from the plate shown in Figure 1. In order to accommodate a wide range of stellar magnitudes, one needs a function that changes shape with brightness. We obtained good results with a function presented by Stetson (1979),

$$d_{\rm S}(x,y) = [d_{\rm G}(x,y)^{-q} + d_{\rm sat}^{-q}]^{-1/q}, \qquad (4)$$

where $d_{\rm sat}$ is the saturation level of the plate and q describes the sharpness of the transition to saturation. This function has the desirable limits $d_{\rm S} \to d_{\rm G}$ for $d_{\rm G} \ll d_{\rm sat}$, and $d_{\rm S} \to d_{\rm sat}$ for $d_{\rm G} \gg d_{\rm sat}$. It is specified by nine parameters: x_0 and y_0; $d_{\rm sky}$ and $d_{\rm peak}$; σ_x, σ_y, and ρ; and the saturation parameters $d_{\rm sat}$ and q.
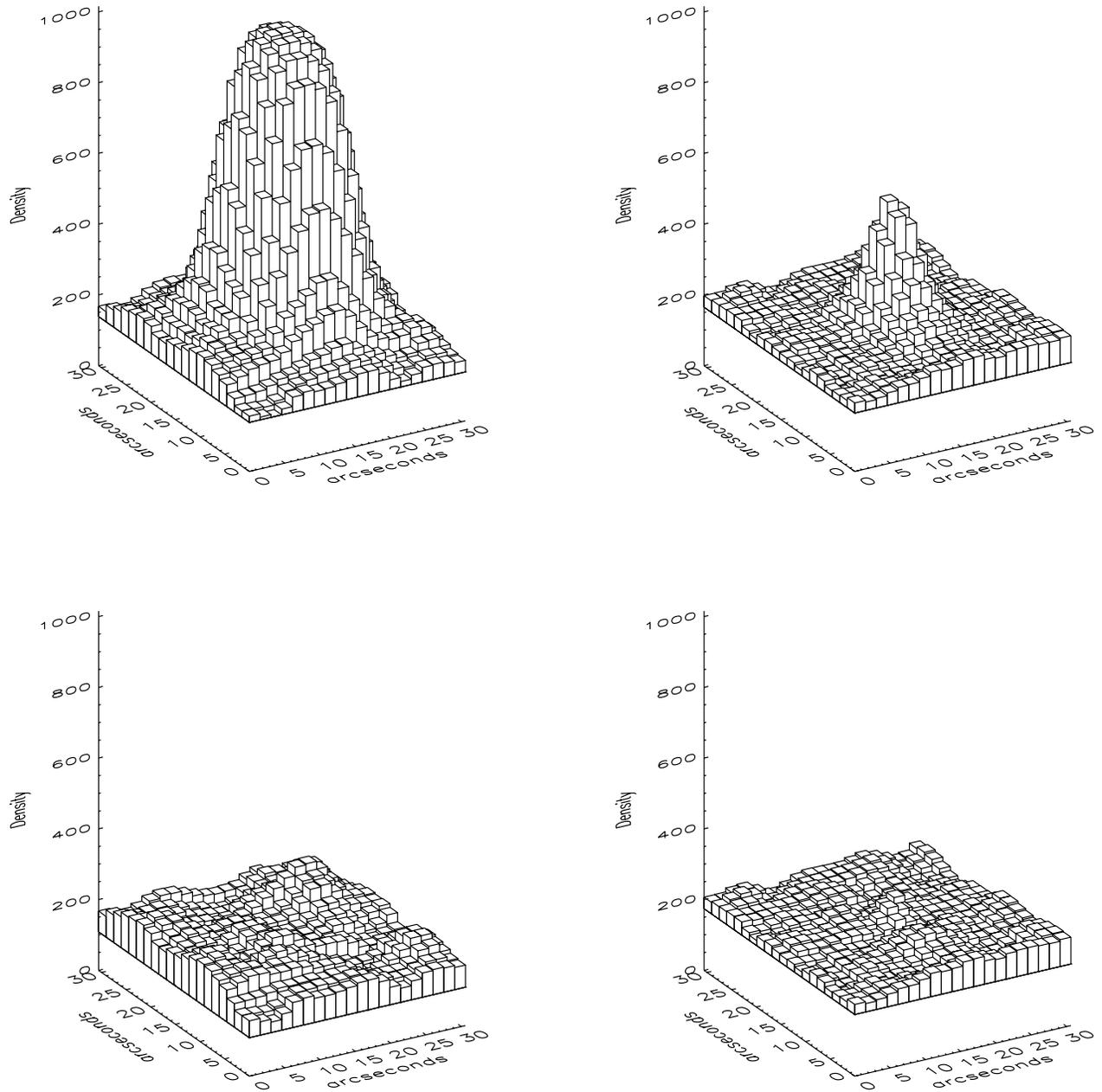
Fig. 2.—Example density distributions from the plate shown in Fig. 1. The top panels show a bright star (*left*) and KH 15D (*right*). The bottom panels show the residuals after subtracting the point-spread function model (eq. [4]).

The bottom two panels of Figure 2 show the residuals after fitting equation (4) to the two example stars. In both cases the fit is excellent. For the range of stellar brightnesses considered in this paper, the peak residual was always ≲10% of the peak value of the density distribution. After fitting each star, we used the best-fitting values of the parameters to compute

$$S \equiv d_{\mathrm{peak}} \sigma_x \sigma_y, \qquad (5)$$

which is proportional to the volume of the density distribution above the sky level, in the limit $d_{\mathrm{sat}} \to \infty$. By computing S in this manner, we attempt to correct for saturation and provide a quantity that is easily related to total stellar flux.

We selected 163 preliminary reference stars from the Flaccomio et al. (1999, hereafter F99) catalog of *BVRI* CCD photometry of NGC 2264. Our selection criteria were that the stars should fall within the $20' \times 20'$ square region centered on HD 47887, lack close neighbor stars, and span a range of magnitudes ($12.5 < I < 16$) and colors ($0.5 < V-I < 3.0$) bracketing KH 15D ($I = 14.4$, $V-I = 1.6$).

For each star on each plate, we performed a nonlinear least-squares fit of equation (4) to the 20×20 pixel ($\approx 30'' \times 30''$) region surrounding the centroid of the density function. At first, the "plate parameters" q, d_{sat}, σ_x, σ_y, and ρ were determined independently for each star on a given plate. Then each plate parameter was fixed at the median of the values obtained for all stars on that plate, and the stellar fits were recomputed without varying the plate parameters. Finally, we computed S for each star.

In practice, we found that KH 15D and many reference stars were well described by the simple Gaussian function (eq. [2]).
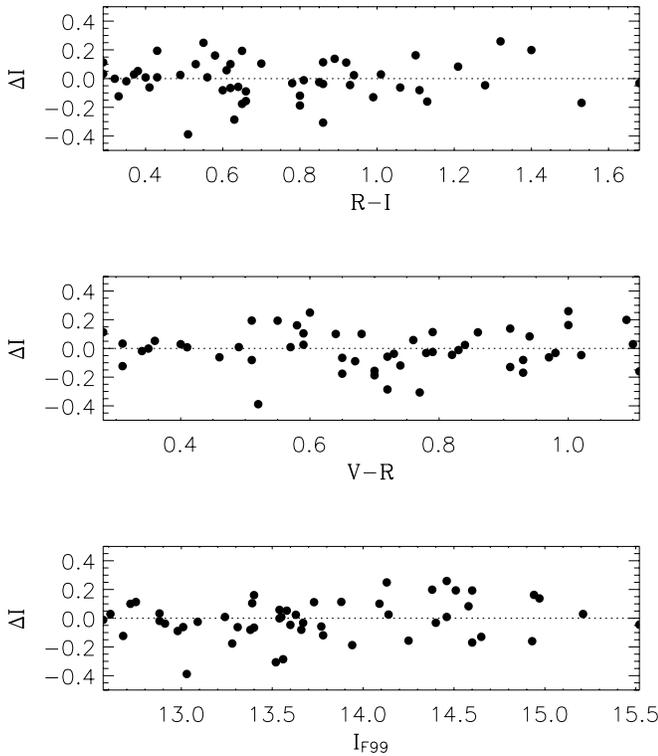
FIG. 3.—Differences between fitted I magnitudes and catalog (F99) I magnitudes, as a function of F99 magnitude and colors. There are no significant correlations between the residuals and either color or magnitude, which is why we did not include color terms or higher order nonlinear terms in eq. (6).

The results reported in this paper are based on the analysis using equation (4), but we also repeated the analysis with the Gaussian function after dropping the brightest reference stars. None of our conclusions changed significantly.

3.2. Reduction to Standard Magnitudes

Next we sought the relationship between S and standard magnitudes. For the I-N/RG 5 plates, we converted S into Cousins I using the relation

$$I = I_0 - 2.5(1 + \epsilon) \log S, \qquad (6)$$

where ϵ represents the nonlinearity: the stellar flux is proportional to $S^{1+\epsilon}$. For each plate, we determined the values of I_0 and ϵ that minimized the sum of squared residuals between the fitted magnitudes and the F99 magnitudes. We experimented with higher order nonlinear terms, and with color terms, but found that these were unhelpful. The residuals show no significant correlation with either magnitude or color (see Fig. 3). For most of the plates, ϵ was about 0.3.

Many of the reference stars are cluster members, which, as young stars, are likely to be variable. At this stage, we culled the most highly variable stars from the list. We computed the standard deviation σ_I of each I-band time series and rejected 110 stars with $\sigma_I > 0.2$ mag. The remaining 53 stars were the final set of reference stars used to determine the magnitude of KH 15D. The choice of 0.2 mag is somewhat arbitrary; increasing the cutoff to 0.3 mag doubles the number of reference stars but has no systematic effect on the derived magnitudes of KH 15D.

Figure 4 is a color-magnitude diagram of the 53 reference stars and KH 15D, showing that KH 15D is bracketed in both

color and magnitude. For each reference star, Table 1 gives the F99 catalog number, F99 I magnitude, the mean I magnitude measured in the Asiago plates, the difference between those two magnitudes, and σ_I.

For the three 103a-E/RG 1 plates, we used the same set of 53 reference stars to convert S into Johnson R band, using a relation analogous to equation (6). Likewise, for the single 103a-O/GG 5 plate, we converted S into Johnson B. The entries for these plates in Table 2 are estimates of I under the assumption that the colors of KH 15D were $R-I = 0.80$ and $B-I = 2.92$, as measured by F99 (see also § 4.4).

3.3. Estimation of Errors

Figure 5 is a plot of σ_I versus the time-averaged I magnitude for all the reference stars. We interpret the lower envelope of the points in Figure 5 as the limiting uncertainty of our relative I-band measurements, as a function of magnitude. Reference stars for which σ_I is much larger than this envelope are presumably variable stars. A reasonable approximation of the lower envelope is

$$\log \sigma_{I,\min}(I) = -1.05 + 0.144(I - 14.4), \qquad (7)$$

which is plotted as a dashed line in Figure 5.

The uncertainty in a single measurement on a given plate may be different from $\sigma_{I,\min}$, depending on the quality of that plate. One measure of plate quality is σ_m, the standard deviation of residuals to the fit of equation (6), in magnitudes. We supposed that the uncertainty is proportional to σ_m. Thus, for a star with magnitude I measured on a plate with fit error σ_m, we estimated the uncertainty to be

$$\text{unc.} = \sigma_{I,\min}(I)\left(\frac{\sigma_m}{\sigma_{m,\min}}\right), \qquad (8)$$

where $\sigma_{m,\min}$ is the minimum value of σ_m among all the plates. For the three R-band measurements and the single B-band measurement, for which a long time series was not available, we used σ_m as the estimate of uncertainty.

4. RESULTS

The resulting I-band magnitudes of KH 15D are given in Table 2. Figure 6 shows the I-band light curve, in which there
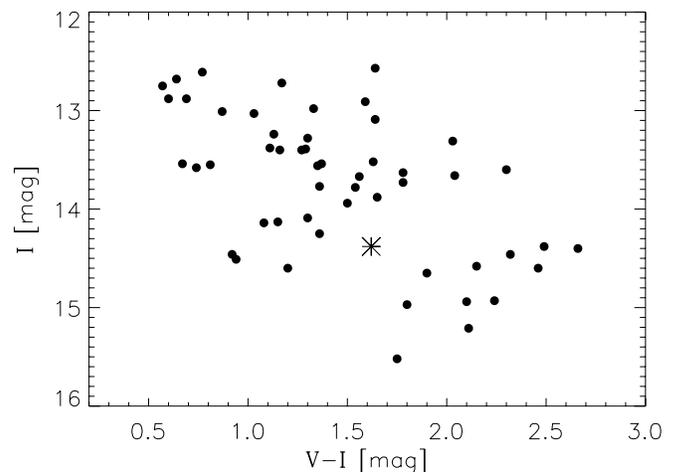

FIG. 4.—Color-magnitude diagram for the 53 reference stars (circles), and KH 15D (asterisk). Data taken from F99.

F99 Catalog No.	I_{F99}	I_{Asiago}[a]	ΔI[b]	σ_I
113................................	15.52	15.51	0.01	0.24
122................................	14.51	14.44	0.07	0.11
128................................	14.60	14.48	0.12	0.09
160................................	14.13	13.85	0.28	0.08
165................................	13.54	13.50	0.04	0.06
173................................	14.65	14.59	0.06	0.12
195................................	13.38	13.48	−0.10	0.09
208................................	13.73	13.70	0.03	0.07
227................................	13.39	13.30	0.09	0.11
263................................	13.40	13.29	0.11	0.06
272................................	12.57	12.57	0.00	0.06
281................................	13.60	13.58	0.02	0.05
289................................	14.94	14.95	−0.01	0.16
297................................	14.40	14.44	−0.04	0.11
305................................	13.31	13.32	−0.01	0.09
315................................	13.28	13.43	−0.15	0.06
320................................	12.88	12.94	−0.06	0.06
321................................	13.03	13.33	−0.30	0.12
338................................	13.58	13.57	0.01	0.06
342................................	13.94	14.10	−0.16	0.11
346................................	14.60	14.64	−0.04	0.11
353................................	13.63	13.63	0.00	0.06
364................................	15.21	15.27	−0.06	0.12
374................................	13.52	13.75	−0.23	0.11
378................................	14.25	14.33	−0.08	0.08
381................................	13.09	13.12	−0.03	0.06
385................................	12.91	12.96	−0.05	0.06
404................................	14.97	14.79	0.18	0.14
409................................	13.88	13.74	0.14	0.08
411................................	14.38	14.26	0.12	0.09
419................................	13.77	13.91	−0.14	0.18
422................................	13.66	13.67	−0.01	0.09
424................................	13.78	13.79	−0.01	0.06
426................................	13.56	13.72	−0.16	0.08
430................................	14.93	14.97	−0.04	0.14
431................................	13.01	12.97	0.04	0.07
432................................	14.46	14.38	0.08	0.08
434................................	12.98	13.07	−0.09	0.06
440................................	13.67	13.63	0.04	0.08
443................................	14.46	14.31	0.15	0.08
444................................	12.72	12.70	0.02	0.06
450................................	14.09	14.02	0.07	0.06
451................................	12.75	12.70	0.05	0.05
452................................	14.58	14.45	0.13	0.10
453................................	12.61	12.65	−0.04	0.06
460................................	13.24	13.22	0.02	0.07
462................................	13.54	13.48	0.06	0.05
463................................	12.88	12.79	0.09	0.06
481................................	13.40	13.45	−0.05	0.07
504................................	13.55	13.53	0.02	0.06
512................................	14.14	14.15	−0.01	0.10
515................................	12.68	12.78	−0.10	0.07

[a] Time average from all plates.
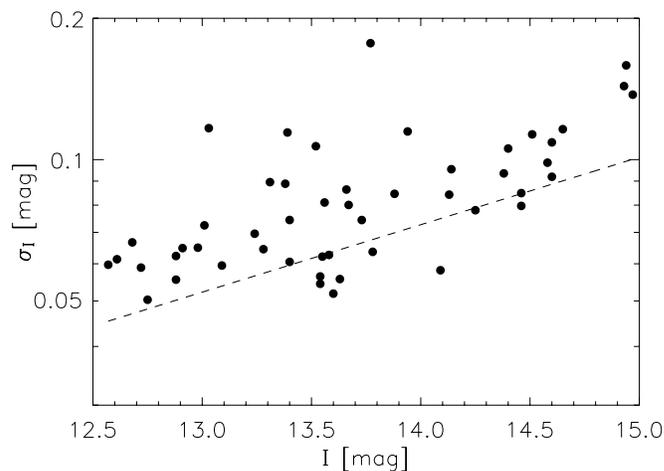[b] $\Delta I = I_{F99} - I_{Asiago}$.

FIG. 5.—The rms scatter in the time series of each standard star, as a function of mean I magnitude. The dashed line is our approximation $\sigma_{I,min}(I)$ for the lower envelope.

days; Herbst et al. 2002). To estimate the statistical uncertainty in our period determination, we used a Monte Carlo procedure. Assuming the measurement errors are Gaussian with standard deviations given by the recipe of § 3.3, we generated 10^4 statistical realizations of the I-band light curve and determined the peak value of the periodogram in each case. The resulting distribution of periods had a standard deviation of 0.02 days. Thus, both our period and the modern period have a formal uncertainty of $\sigma = 0.02$ days and differ by 3.5 σ, or 1.75 σ in each period. This may indicate a discrepancy, but it is also quite possible that our Monte Carlo procedure underestimates the true uncertainty, as a result of the time evolution of the light curve.

We computed the phase of each observation,

$$\phi = \frac{(JD - J_0) \bmod P}{P}, \qquad (9)$$

where JD is the Julian Date of the observation, $P = 48.35$ days, and $J_0 = 2,452,690.67$, taken from the most recent ephemeris (Hamilton 2004). Figure 8 shows the phased light curve. For comparison, we have also plotted CCD-based measurements from 2001 to 2002, kindly provided by C. Hamilton.

4.2. Brightness Variations

In the Asiago light curve, the star alternates periodically between a bright state and a faint state. The fading events last ≈20 days, which is about the same duration as the 2000–2001 eclipses. However, the fractional variation in flux is much smaller in the Asiago light curve. The difference between the average magnitude in the bright state (defined as $-0.30 \leq \phi \leq 0.10$) and the faint state ($0.25 \leq \phi \leq 0.55$) is $\Delta I = 0.67 \pm 0.07$ mag. By contrast, the modern eclipse depth is 3.5 mag. Interestingly, the three faintest measurements are also from the most recent time series (1979–1982; Fig. 8, asterisks), which is consistent with a progressive deepening of the eclipses.

4.3. Magnitude of the Bright State

The mean magnitude of the bright state in the Asiago light curve is $I = 13.57 \pm 0.03$, as compared with 14.47 ± 0.03 for the modern data. The bright state was formerly 0.90 mag

are significant variations. In the following sections we compare the Asiago light curve with the modern light curve.

4.1. Periodicity

The brightness variations were periodic in the past, as they are today. A Lomb-Scargle periodogram of the I-band light curve (Fig. 7) shows a highly significant peak at a period of 48.42 days, which is close to the modern period (48.35 ± 0.02

TABLE 2
Photometric Measurements of KH 15D

JD	ϕ^a	I	JD	ϕ^a	I	JD	ϕ^a	I
2,439,530.46............	0.8121	13.46 ± 0.08	2,439,878.48...........	0.009931	13.5 ± 0.1	2,440,588.51..........	0.6951	13.64 ± 0.09
2,439,763.22............	0.6261	13.43 ± 0.08	2,439,878.52...........	0.01074	13.45 ± 0.09	2,440,589.58..........	0.7172	13.5 ± 0.1
2,439,765.65............	0.6762	13.7 ± 0.1	2,439,879.30...........	0.02694	13.47 ± 0.09	2,440,621.55..........	0.3785	14.3 ± 0.1
2,439,769.65............	0.7591	13.45 ± 0.08	2,439,881.51...........	0.07251	13.5 ± 0.1	2,440,626.32..........	0.4772	14.3 ± 0.1
2,439,771.58............	0.7989	13.5 ± 0.1	2,439,885.53...........	0.1556	13.82 ± 0.09	2,440,647.35..........	0.9121	13.6 ± 0.2
2,439,772.56............	0.8192	13.47 ± 0.09	2,439,887.50...........	0.1965	13.9 ± 0.1	2,441,960.64..........	0.07422	13.6 ± 0.1
2,439,773.59............	0.8405	13.5 ± 0.1	2,439,905.46...........	0.5680	13.7 ± 0.1	2,442,373.51..........	0.6135	14.0 ± 0.2[b]
2,439,774.62............	0.8619	13.44 ± 0.09	2,439,943.30...........	0.3506	14.0 ± 0.1	2,442,396.49..........	0.08877	13.4 ± 0.2[b]
2,439,774.67............	0.8628	13.5 ± 0.1	2,439,947.31...........	0.4335	14.0 ± 0.1	2,442,397.49..........	0.1093	13.3 ± 0.2[c]
2,439,775.63............	0.8826	13.49 ± 0.09	2,440,127.66...........	0.1636	13.7 ± 0.1	2,442,397.50..........	0.1095	13.6 ± 0.2[b]
2,439,796.57............	0.3157	14.09 ± 0.08	2,440,241.49...........	0.5178	13.73 ± 0.09	2,442,816.44..........	0.7744	13.60 ± 0.08
2,439,826.67............	0.9384	13.6 ± 0.1	2,440,264.25...........	0.9886	13.65 ± 0.08	2,444,202.51..........	0.4418	14.6 ± 0.2
2,439,827.66............	0.9588	13.5 ± 0.1	2,440,273.28...........	0.1753	13.9 ± 0.1	2,444,292.42..........	0.3013	14.4 ± 0.2
2,439,831.69............	0.04213	13.7 ± 0.1	2,440,274.44...........	0.1994	14.0 ± 0.1	2,444,609.31..........	0.8555	13.7 ± 0.1
2,439,852.63............	0.4753	14.1 ± 0.1	2,440,479.66...........	0.4439	14.3 ± 0.1	2,444,642.49..........	0.5417	14.5 ± 0.2
2,439,860.58............	0.6396	13.60 ± 0.08	2,440,485.66...........	0.5679	14.0 ± 0.1	2,445,002.48..........	0.9872	13.8 ± 0.1
2,439,876.33............	0.9655	13.50 ± 0.09	2,440,509.67...........	0.06442	13.9 ± 0.1			
2,439,877.33............	0.9862	13.53 ± 0.06	2,440,569.55...........	0.3030	14.3 ± 0.1			

[a] Phase calculated assuming a 48.35 day period.
[b] From 103a-E/RG 1 plate. I was estimated assuming $R-I = 0.80$.
[c] From 103a-O/GG 5 plate. I was estimated assuming $B-I = 2.92$.

(2.3 times) brighter than it is today. One might reasonably wonder whether this surprising discrepancy is due to an error in the zero point of our magnitude relation, or a systematic effect such as contamination by scattered light from HD 47887.

Regarding the accuracy of the zero point, Figure 9 shows a histogram of ΔI, the differences between the time-averaged magnitudes of the 53 reference stars in the Asiago plates, and the corresponding F99 magnitudes. More than 67% of the stars have $\Delta I < 0.1$ mag, and the maximum ΔI is 0.3 mag. This gives us confidence that the zero point is accurate to ≈ 0.15 mag.

Regarding possible contamination, the I-N/RG 5 plates were chosen precisely to minimize this problem. In the top right panel of Figure 2, the halo of HD 47887 is evident as a small gradient in the sky level surrounding KH 15D. This gradient is too small to cause a 0.9 mag (230%) error in the estimate of the volume beneath the peak. Star 385 is even closer to HD 47887 (see Fig. 1) and has $\Delta I = -0.05$ mag. Star 404 is

also within the halo of scattered light and has $\Delta I = 0.18$ mag, despite being a known variable star (Kukarkin et al. 1971).

4.4. Color Variation

It would be interesting to know whether the decrease in overall brightness was accompanied by a color change. We have very limited color information, having concentrated on the I-N/RG 5 plates, but the few bluer plates in our sample show no evidence for a color change. In particular, we obtained estimates of B and R from plates exposed less than 1 hr apart on 1974 December 15 (JD 2,439,774.6; see Table 2). The phase on this date was $\phi = 0.11$, corresponding to the transition from the bright state to the faint state. The result was $B-R = 2.0 \pm 0.3$, in agreement with the F99 measurement, $B-R = 2.14$.

4.5. Phase of Minimum Light

In the 30 years between the earliest group of Asiago observations and the determination of the Herbst et al. (2002)

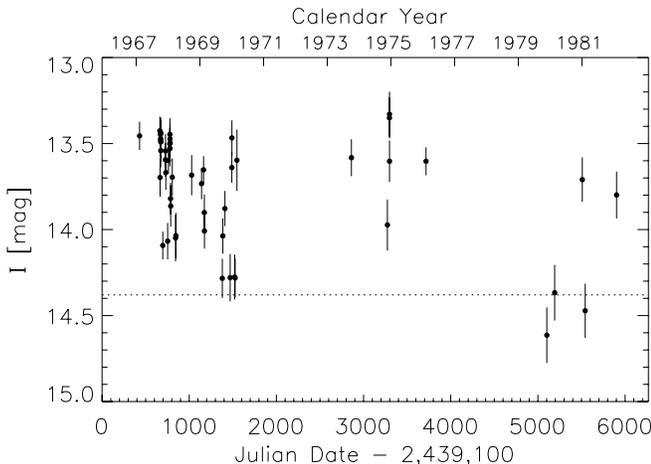

Fig. 6.—The I-band light curve of KH 15D from the Asiago plates. The dotted line marks the magnitude of the bright state as observed today. The error bars were computed with eq. (8).
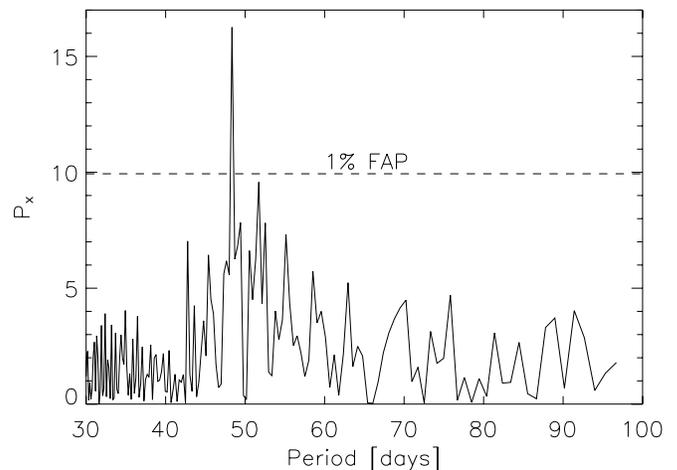

Fig. 7.—Lomb-Scargle periodogram of the light curve shown in Fig. 6. Peaks above the dashed line have a less than 1% chance of being a false alarm.
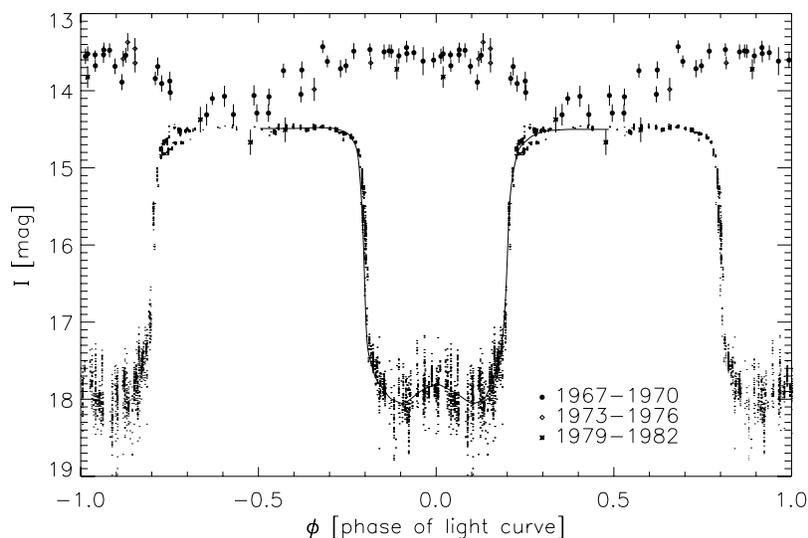
FIG. 8.—Phased light curve of KH 15D from 1967–1982 (*large symbols*) and 2001–2002 (*dots*). The solid line is a B-spline interpolation of the 2001–2002 data (see § 5).

ephemeris, there have been more than 200 eclipses. The 0.02 day uncertainty in each period causes a phase uncertainty of $\Delta\phi \approx 0.1$ in the connection between the modern light curve and the Asiago light curve. Yet the phase of minimum light in the Asiago light curve occurs at $\phi_m = 0.4$, rather than $\phi_m = 0$ as in the modern light curve. This implies, at the 4 σ level, that there has been a shift in the phase of minimum light.

An important caveat, as mentioned in § 4.1, is that period determination for this system is difficult because the light curve does not repeat exactly from period to period. We believe it is reasonable that the period uncertainty has been underestimated, despite our best effort and the best effort of Herbst et al. (2002). This makes us reluctant to attach too much significance to the apparent phase shift before this point is clarified with additional archival data or continued monitoring.

5. SUMMARY AND DISCUSSION

The fading events of KH 15D were occurring between 1967 and 1982 with nearly the same period and duration as observed today. However, the system has changed over the past 30 years in two major respects. First, the bright state has decreased in flux by a factor of 2.3 (0.9 ± 0.1 mag). Second, the contrast between the bright state and the faint state has increased dramatically. Formerly, the flux of the faint state was 54% of the flux of the bright state ($\Delta I = 0.67 \pm 0.07$ mag). In modern observations, the corresponding figure is 4% (3.5 mag).

Interestingly, these two observations could both be explained by a time-independent flux that was present during the Asiago observations and not present during the modern observations. A steady light source with 1.3 times the flux of the eclipsing K7 star would increase the total flux by a factor of 2.3 and would also dilute the eclipses. When the K7 star is totally eclipsed, the total flux would be reduced to 1.3/2.3 = 57% of the bright state.

To elaborate upon this idea, we created a smooth model of the 2000–2001 light curve using B-spline interpolation. This model is shown as a solid line in Figure 8. Then we considered three possible transformations of the model light

curve: (1) add a constant light source of magnitude I_0; (2) shift the phase by $\Delta\phi$; and (3) stretch or compress the eclipse duration by a factor R. We determined the values of I_0, $\Delta\phi$, and R that provide the best match to the Asiago light curve, using a nonlinear least-squares algorithm. The best fit was obtained for $I_0 = 14.11$, $\Delta\phi = 0.38$, and $R = 0.9$. In Figure 10, the transformed modern light curve is superposed on the Asiago data, and the residuals are plotted beneath the data. The rms scatter of the residuals is 0.17 mag and the reduced χ^2 is 2.1.

The success of this simple model leads us to hypothesize that there is a second star in the KH 15D system. The second star was formerly blended with the $I = 14.4$ K7 star seen today but is now completely obscured. This provides an appealing explanation of the Asiago light curve but does raise an obvious question: where did the second star go?

The most economical answer, in the sense that it requires the fewest new complexities, is that the second star is currently behind the same opaque material that causes the periodic eclipses of the K7 star. The composition and arrangement
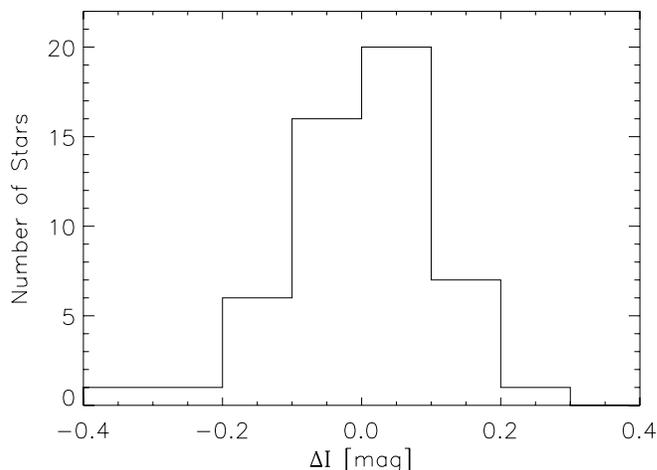

FIG. 9.—Histogram of differences between mean I magnitudes from the Asiago plates and catalog I magnitudes (F99) for the 53 reference stars. The distribution is centered near zero and has standard deviation 0.14.
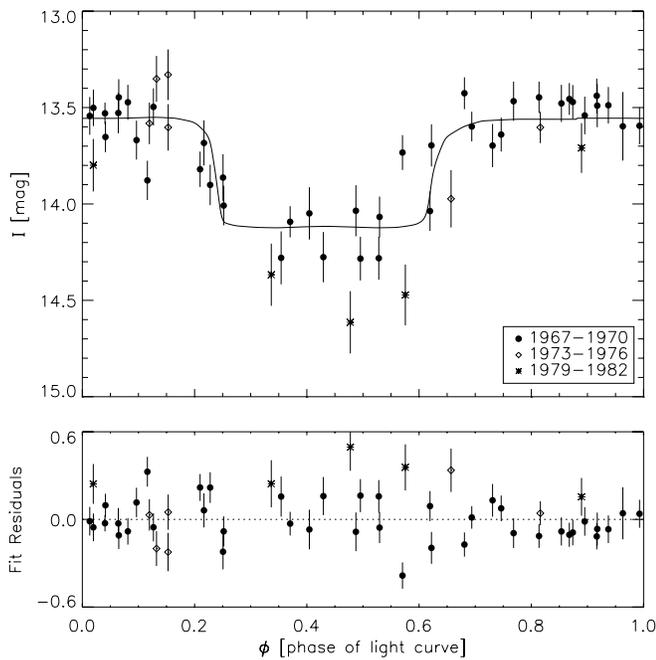
FIG. 10.—Phased light curve of KH 15D from 1967 to 1982, with a model based on a transformation of the 2000–2001 phased light curve (see § 5). The residuals (model minus data) are plotted beneath the light curve.

of that material are unknown. Some theories are a nearly edge-on circumstellar or protoplanetary disk (Hamilton et al. 2001; Herbst et al. 2002; Winn et al. 2003; Agol et al. 2004), a dusty banana-shaped vortex (Barge & Viton 2003), and a cometary distribution of accreting material around a low-mass companion (Grinin & Tambovtseva 2002). The material might be distributed in such a way that one star is always hidden and the other star comes into view periodically, as a result of the orbital motion of the star or the circumstellar material.

If the system is truly a binary, one would expect to see radial velocity variations. Assuming the observed K7 star has a mass of $\approx 0.6\ M_\odot$, as estimated by Hamilton et al. (2001), and that it is in a 48 day edge-on orbit with a star of similar mass, its orbital velocity would be ≈ 30 km s^{-1}. This is 10 times larger than the velocity shift measured by Hamilton

et al. (2003) between two widely separated phases. Of course, it is possible that the full radial velocity curve shows larger variations. It is also possible that the second star is a wide binary companion, an unrelated background or foreground star, or a binary companion in a nearly face-on orbit.

Allowing for the possibility of a second star to the system does not, by itself, explain the eclipses or their evolution. However, our discovery that KH 15D was brighter in the past puts two of the previous observations of this system in a different light. One of these is the result of the 1913–1951 Harvard plate analysis. Winn et al. (2003) derived limits on the fraction of time that the eclipses were greater than 1 mag, but this ignored the possibility that the system was brighter at *all* phases in the past. The more precise statement of the result is that the system was rarely more than 1 mag fainter than the *modern* bright state. More speculatively, there may be a connection to the surprising observation by Kearns & Herbst (1998) that during a few of the rebrightening events, the system became *brighter* than the usual bright state by 0.1–0.5 mag. Perhaps during these events we were allowed a peek at the second star.

With the Asiago plates, we have discovered several new clues regarding the mysterious eclipses of KH 15D, demonstrating the value of long-term preservation of astronomical images. It will be interesting to extend the historical analysis with additional plates from the 1980s and 1990s, to reveal when and how the extra light source turned off, and to complete the connection with modern data.

---

[6] See http://www.skyarchive.org.

REFERENCES

Agol, E., Barth, A. J., Wolf, S., & Charbonneau, D. 2004, ApJ, 600, 781
Barbieri, C., Omizzolo, A., & Rampazzi, F. 2003, Mem. Soc. Astron. Italiana, 74, 430
Barge, P., & Viton, M. 2003, ApJ, 593, L117
Flaccomio, E., Micela, G., Sciortino, S., Favata, F., Corbally, C., & Tomaney, A. 1999, A&A, 345, 521 (F99)
Grinin, V. P., & Tambovtseva, L. V. 2002, AZh Pisma, 28, 667 (English transl. Astron. Lett., 28, 601)
Hamilton, C. M. 2004, in preparation
Hamilton, C. M., Herbst, W., Mundt, R., Bailer-Jones, C. A. L., & Johns-Krull, C. M. 2003, ApJ, 591, L45
Hamilton, C. M., Herbst, W., Shih, C., & Ferro, A. J. 2001, ApJ, 554, L201
Herbst, W., et al. 2002, PASP, 114, 1167

Herbst, W., Herbst, D. K., Grossman, E. J., & Weinstein, D. 1994, AJ, 108, 1906
Kearns, K. E., & Herbst, W. H. 1998, AJ, 116, 261
Kukarkin, B. V., Kholopov, P. N., Pskovsky, Yu. P., Efremov, Yu. N., Kukarkina, N. P., Kurochkin, N. E., & Medvedeva, G. I. 1971, General Catalogue of Variable Stars (3rd ed.; Moscow: Nauka)
Moro, D., & Munari, U. 2000, A&AS, 147, 361
Stetson, P. B. 1979, AJ, 84, 1056
Stock, J., & Williams, A. D. 1962, in Stars and Stellar Systems, Vol. 2, Astronomical Techniques, ed. W. A. Hiltner (Chicago: Univ. Chicago Press), 374
Winn, J. N., Garnavich, P. M., Stanek, K. Z., & Sasselov, D. D. 2003, ApJ, 593, L121